A hybrid controller for ABS based on extended-braking-stiffness estimation

Missie Aguado-Rojas, William Pasillas-Lépine, Antonio Loria

A hybrid controller for ABS based on extended-braking-stiffness estimation ⋆

Missie Aguado-Rojas * **William Pasillas-Lépine** ** **Antonio Loría** **

* *Université Paris-Sud, Université Paris-Saclay, L2S-CentraleSupélec, 91192 Gif-sur-Yvette, France*
** *CNRS, L2S-CentraleSupélec, 91192 Gif-sur-Yvette, France*
(e-mails: {missie.aguado}{pasillas}{loria}@l2s.centralesupelec.fr)

Abstract: In the context of antilock braking systems (ABS), we present a two-phase hybrid control algorithm based on the tyre extended braking stiffness (XBS), that is, on the slope of the tyre-road friction coefficient with respect to the wheel slip. Because the XBS cannot be directly measured, a switched observer is used to estimate it. With the proposed hybrid algorithm, the closed-loop trajectories of the system satisfy the conditions required for the observer to correctly estimate the XBS. Moreover, the braking distances are shorter than those obtained using a hybrid algorithm based on wheel deceleration thresholds.

Keywords: ABS; braking distance; switched systems; persistency of excitation;

1. INTRODUCTION

Introduced by Bosch in 1978 for production passenger cars, the antilock braking system (ABS) is the core of today's active driving-safety systems. Its main objectives are to prevent the wheels from locking in order to maintain the stability and steerability of the vehicle during heavy braking, and to maximally exploit the tyre-road friction coefficient in order to achieve the shortest possible braking distance [Corno et al., 2012; Singh et al., 2013].

Most commercial ABS use a regulation logic based on wheel deceleration thresholds (see, e.g. Kiencke and Nielsen [2005]; Gerard et al. [2012]; Reif [2014]). The principle of these algorithms is based on generating limit cycles in a desired range of longitudinal wheel slip. The main force of these controllers is that they are able to keep wheel slip in a neighborhood of the optimal point without using explicitly its value and they are quite robust with respect to changes in tyre parameters and road conditions. Their main drawback, however, is that they are often based on purely heuristic arguments and the tuning of the deceleration thresholds is not an easy task [Choi, 2008; Hoàng et al., 2014]. Moreover, the wheel-slip cycling range cannot be explicitly chosen; instead, it has to be selected indirectly through the wheel deceleration thresholds. The objective of this paper is to design an algorithm that allows the cycling range to be chosen in a more direct manner. To that end, we present a regulation logic based on the tyre extended braking stiffness (XBS).

The braking stiffness is the slope of the tyre-road friction curve with respect to the wheel slip at the zero-friction operating point [Gustafsson, 1997]. As a generalization of this concept, the XBS may be defined as the slope of the friction-vs-slip curve at *any* operating point [Sugai et al., 1999; Umeno, 2002]. The interest of using the XBS is that, in contrast to the unknown optimal value of wheel slip, the optimal value of XBS is always known and equal to zero. Hence, the (control) objective of an ABS algorithm may be reformulated in terms of this variable. In other words, our objective is to design an algorithm such that the XBS remains in a neighbourhood around zero.

The concept of maximizing the braking force in an ABS based on the XBS was introduced by Sugai et al. [1999], and was later extended by Umeno [2002] and Ono et al. [2003]. In these works, however, the XBS is implicitly assumed to be a constant parameter so its dynamics is neglected. In Villagra et al. [2011], in order to estimate the maximum friction coefficient, the XBS is used to signal the entrance of the tyre into a different road surface and to distinguish one type of road from another. In Hoàng et al. [2014] the XBS is used to perform closed-loop wheel acceleration control during some phases of a five-phase wheel-deceleration-based algorithm.

In this paper, a two-phase algorithm based on XBS thresholds is developed. This work builds upon the results presented in Aguado-Rojas et al. [2018], where an observer to estimate the XBS under unknown road conditions was introduced. By directly choosing the values of XBS thresholds, the proposed algorithm allows an easier and more direct selection of the wheel-slip cycling range and, consequently, to reduce the braking distance. Moreover, it is shown that the trajectories of the system satisfy the conditions required for the observer to correctly estimate the XBS, which may not be achieved with continuous control algorithms.

2. XBS DYNAMICS

Consider a quarter-car model composed of a wheel with radius R and angular velocity ω mounted on a vehicle with longitudinal velocity v_x. The normalized relative velocity between the vehicle and the tyre, known as the wheel slip

⋆ The work of the first author is supported by CONACYT, Mexico.

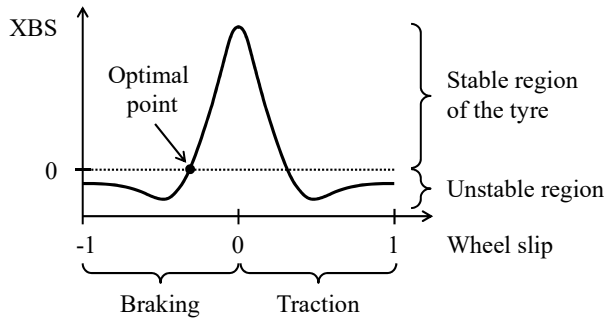

Fig. 1. Typical shape of the XBS-vs-slip curve.

$$\lambda = \big(R\omega - v_x\big)/v_x,$$

determines the friction coefficient μ between the tyre and the road through a nonlinear relation $\mu(\lambda)$.

Define as state variables the wheel acceleration offset

$$z_1 := R\dot{\omega} - \dot{v}_x(t),$$

that is, the difference between the longitudinal acceleration of the vehicle and the linear acceleration of the tyre at the wheel-ground contact point, and

$$z_2 := \mu'(\lambda),$$

that is, the tyre extended braking stiffness (XBS). The shape of the curve $\mu'(\lambda)$ is illustrated in Fig. 1. The point at which the maximum braking force can be obtained corresponds to $z_2 = 0$. The area above this point is called the stable region of the tyre, and the area below is called the unstable region. Given a suitable choice for the tyre-road friction $\mu(\lambda)$, a simple second-order model in which the XBS appears directly as a state variable can be developed. In this work the friction model proposed by Burckhardt [1993] is used, hence the XBS is modelled as

$$\mu'(\lambda) = c_1 c_2 \exp(-c_2\lambda) - c_3,$$

where the coefficients c_i are constants that depend on the road conditions.

During an ABS braking scenario, $\dot{v}_x(t)$ remains almost constant and close to the maximal value allowed by the road conditions, while λ remains relatively small. Under such conditions, the dynamics of z_1 and z_2 are described by [1]

$$\dot{z}_1 = -\frac{a}{v_x(t)} z_1 z_2 - bu \tag{1a}$$

$$\dot{z}_2 = \big(cz_2 + d\big)\frac{z_1}{v_x(t)} \tag{1b}$$

$$y = z_1, \tag{1c}$$

where the control input u is the derivative of the brake pressure, the measured output y is the wheel acceleration offset, the positive parameters a and b depend on the geometrical characteristics of the wheel, and c and d on the road conditions. All parameters are assumed to be known and constant. The vehicle speed $v_x(t)$ is considered as a known external variable and assumed to be positive, bounded, and bounded away from zero.

The aim of this paper is to design a control law such that the XBS remains close to its optimal value and thus maximize the braking force during an emergency braking scenario.

[1] See Hoàng et al. [2014] and Aguado-Rojas et al. [2018] for the complete derivation of this model.

3. CONTINUOUS CONTROL DESIGN

To simplify the control design, let us assume for the moment that both z_1 and z_2 are known. Under this assumption, one may design a control law that stabilizes system (1) at the origin. Note, however, that because the control input u does not appear explicitly in (1b), one must achieve the objective through z_1, that is, regarding the latter as a virtual control.

Hence, we first design a virtual reference z_1^* such that if $z_1 = z_1^*$, then $z_2 \to z_2^* = 0$. One such reference is

$$z_1^* = -k_r \frac{z_2}{cz_2 + d}, \qquad k_r > 0, \tag{2}$$

since, setting $z_1 = z_1^*$ in (1b) leads to $\dot{z}_2 = -k_r z_2/v_x(t)$ which is exponentially stable.

To perform the tracking of z_1^*, the control is designed as

$$u = \frac{1}{b}\left[-\frac{a}{v_x(t)} z_1 z_2 + \frac{k_p}{v_x(t)}\big(z_1 - z_1^*\big) - \dot{z}_1^*\right], \qquad k_p > 0, \tag{3}$$

where we employ (1b) in the evaluation of $\dot{z}_1^*$. Hence, the latter is implemented using z_1 and z_2 as

$$\dot{z}_1^* = -\frac{k_r}{v_x(t)} \frac{dz_1}{cz_2 + d}.$$

Note that, even though the right-hand side of (2) is not defined when $z_2 = -d/c$, this singularity lies outside the domain in which z_2 is physically feasible. Indeed, there exist $z_2^{\max} \geq z_2 \geq z_2^{\min} > -d/c$. Hence, z_1^* is well-posed.

Now, let $\tilde{z}_1 := z_1 - z_1^*$ and $\tilde{z}_2 = z_2 - z_2^*$. Substitution of (3) in (1a) yields the closed-loop dynamics

$$\dot{z}_1 = \frac{k_p}{v_x(t)}\big(z_1^* - z_1\big) + \dot{z}_1^* = -\frac{k_p}{v_x(t)}\tilde{z}_1 + \dot{z}_1^*$$

and from (1b) and (2) one has

$$\begin{aligned}\dot{z}_2 &= \big(cz_2 + d\big)\frac{z_1^*}{v_x(t)} + \big(cz_2 + d\big)\frac{\tilde{z}_1}{v_x(t)} \\ &= -\frac{k_r}{v_x(t)} z_2 + \big(cz_2 + d\big)\frac{\tilde{z}_1}{v_x(t)}.\end{aligned}$$

Hence, the tracking error dynamics is

$$\dot{\tilde{z}}_1 = -\frac{k_p}{v_x(t)}\tilde{z}_1 \tag{4a}$$

$$\dot{\tilde{z}}_2 = -\frac{k_r}{v_x(t)}\tilde{z}_2 + \frac{c\tilde{z}_2 + d}{v_x(t)}\tilde{z}_1, \tag{4b}$$

which has a cascaded structure. This is relevant because, for cascaded systems, sufficient conditions for the origin to be globally asymptotically stable (GAS) are well established. It is enough that the origin for (4a) be GAS, that the origin for (4b) with $\tilde{z}_1 = 0$ be GAS, and that the solutions of (4) be uniformly globally bounded [Panteley and Loría, 2001].

Now, recalling that $v_x(t)$ is positive, bounded, and bounded away from zero, it follows that the origin of (4a) is GAS. The same holds for the origin of

$$\dot{\tilde{z}}_2 = -\frac{k_r}{v_x(t)}\tilde{z}_2.$$

Moreover, note that because $z_2^* = 0$, the tracking error $\tilde{z}_2 = z_2$ is the XBS itself, which is bounded by nature. Thus, the interconnection term $\big(c\tilde{z}_2 + d\big)/v_x(t)$ is bounded and so are the solutions of (4). Therefore, it follows by a cascade argument that the origin of (4) is GAS.

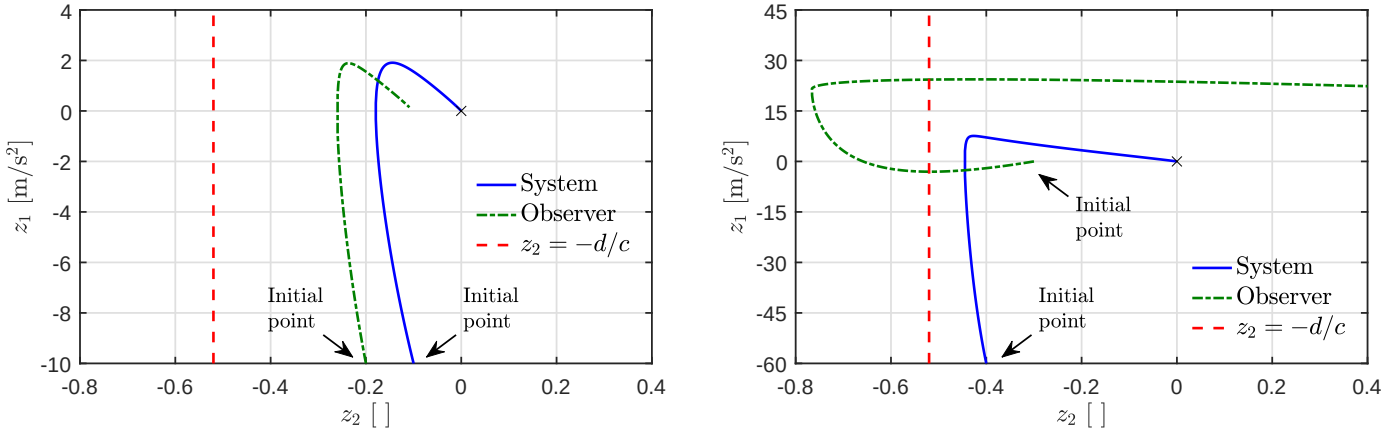

Fig. 2. Continuous state-feedback control: the system converges to the origin. LEFT: The estimated states do not converge to their true values because $z_1 \to 0$ (hence, it is not persistently exciting). RIGHT: During the transient stage, the estimate $\hat{z}_2$ crosses the set $\{cz_2 + d = 0\}$.

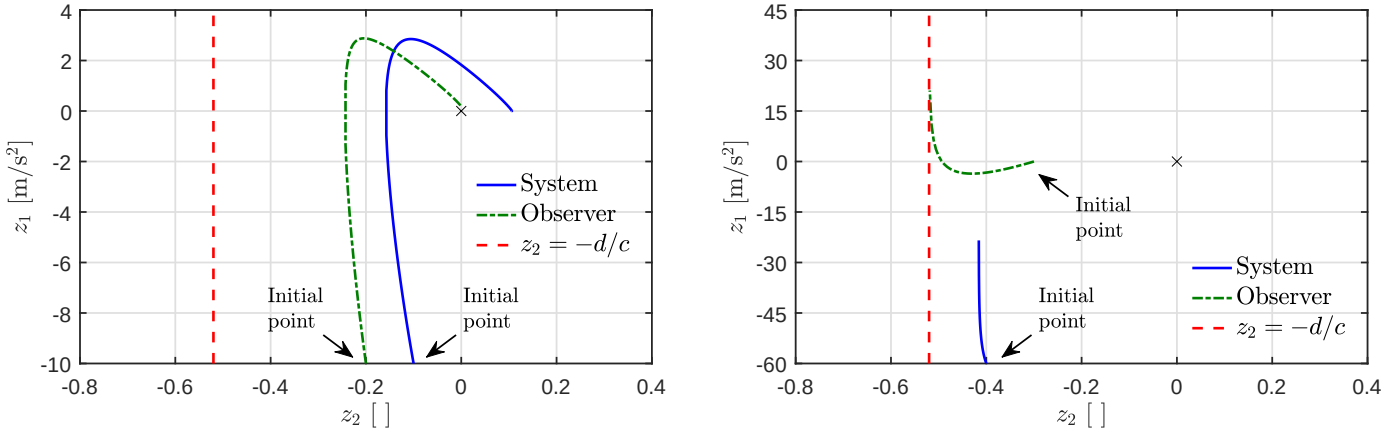

Fig. 3. Continuous output-feedback control using XBS observer: z_2 does not converge to its optimal value. LEFT: The estimated states do not converge to their true values because $z_1 \to 0$ (hence, it is not persistently exciting). RIGHT: Even though the true trajectories of the system remain within the feasible region, as $\hat{z}_2$ approaches $-d/c$, the denominator of the right-hand side of (2) approaches zero and z_1^* grows unbounded. The simulation is stopped when a division by zero is detected.

The performance of this control law is illustrated in Fig. 2. Unless otherwise stated, in what follows we consider a simulation scenario of a vehicle braking on dry asphalt with an initial speed of 90 km/h. The graphics show the evolution of the system (solid line, blue) on the phase-plane for two different initial conditions (the trajectories labeled 'observer' will be discussed later on). Not surprisingly, the control law given by (2) and (3) is able to smoothly steer the system's trajectories towards the origin. We recall, however, that we have momentarily assumed that z_1 and z_2 are known, but in a real-time implementation z_2 cannot be directly measured. Hence, in order to implement the control law, an estimate $\hat{z}_2$ must be used instead. To generate such an estimate, an observer is presented in the following section.

4. XBS OBSERVER

Under the assumptions established in Section 2, an observer for system (1) may be designed as

$$\dot{\hat{z}}_1 = -\frac{a}{v_x(t)} z_1 \hat{z}_2 - bu + k_1(z_1) \frac{z_1}{v_x(t)} \big(z_1 - \hat{z}_1\big) \tag{5a}$$

$$\dot{\hat{z}}_2 = \big(c\hat{z}_2 + d\big) \frac{z_1}{v_x(t)} + k_2(z_1) \frac{z_1}{v_x(t)} \big(z_1 - \hat{z}_1\big), \tag{5b}$$

where

$$k_i(z_1) = \begin{cases} k_i^+ & \text{if } z_1 > 0 \\ k_i^- & \text{if } z_1 < 0 \end{cases} \qquad \text{for } i = \{1, 2\}. \tag{6}$$

Define the estimation errors $\bar{z}_1 := \hat{z}_1 - z_1$ and $\bar{z}_2 := \hat{z}_2 - z_2$. From (1) and (5), one has

$$\begin{bmatrix} \dot{\bar{z}}_1 \\ \dot{\bar{z}}_2 \end{bmatrix} = \frac{z_1}{v_x(t)} \begin{bmatrix} -k_1(z_1) & -a \\ -k_2(z_1) & c \end{bmatrix} \begin{bmatrix} \bar{z}_1 \\ \bar{z}_2 \end{bmatrix}. \tag{7}$$

The observer described by (5) and (6) is a particular case of those presented in Hoàng et al. [2014] and Aguado-Rojas et al. [2018] (in this work the road parameters c and d are assumed to be known, but in the aforementioned references such is not the case). It is a Luenberger-like observer in which the gains $k_i(z_1)$ switch between two different values k_i^+ and k_i^- depending on the sign of z_1. Following the same approach used in those references, it can be shown that if the gains k_i^+ and k_i^- satisfy

$$k_1^+ > c, \quad k_2^+ < -\frac{c}{a}k_1^+, \quad k_1^- < c, \quad k_2^- < -\frac{c}{a}k_1^-, \quad k_1^- = 2c - k_1^+, \quad ck_1^+ + ak_2^+ = ck_1^- + ak_2^-, \tag{8}$$

then the origin of (7) is asymptotically stable, provided that: (i) z_1 is persistently exciting (PE), (ii) z_1 crosses zero only at isolated points, and (iii) any two such points are separated by an interval of length no smaller than $\tau_D > 0$.

The condition (i) holds if there exist positive constants μ_0 and T_0 such that

$$\int_t^{t+T_0} z_1(\varsigma)^2 d\varsigma \geq \mu_0 \qquad \text{for all } t \geq 0. \tag{9}$$

Roughly speaking, (9) means that z_1 should be rich enough to guarantee that the solutions of (7) do not become too slow or remain "stuck" away from zero. The condition (ii) renders the system observable even when it crosses the set $\{z_1 = 0\}$ on which the system is not observable. The conditions (ii) and (iii) imply that there exists a minimal dwell time $\tau_D > 0$ between each consecutive switch of the gains k_i^+ and k_i^-. This three conditions, together with (8), guarantee the asymptotic stability of (7) [Aguado-Rojas et al., 2018].

Fig. 3 illustrates the performance of the control law of Section 3 when (2) and (3) are implemented using $\hat{z}_2$ instead of z_2. In both cases the control fails to drive the system towards the origin. This is caused by two problems: (a) the control law does not guarantee that z_1 is PE because $z_1 \to 0$, and (b) the observer does not guarantee that $\hat{z}_2$ remains within a feasible region for all t. Consider again Fig. 2-Left. The graphic shows the evolution of the observer (dash-dotted line, green) when it is implemented in open loop (that is, independently from the control). In this case, the trajectory of z_1 does not satisfy the persistency of excitation condition so the estimated states do not converge to their true values. When the control is implemented in closed loop with the observer (Fig. 3-Left), this causes the system to converge to a point different than the origin. Now, consider Fig. 2-Right. In this case the estimated states do converge to the true trajectory of the system. However, during the transient stage $\hat{z}_2$ crosses into a region in which such a value of z_2 is not feasible. When the control is implemented in closed-loop with the observer (Fig. 3-Right), the reference z_1^* grows unbounded as $\hat{z}_2$ approaches $-d/c$. When $\hat{z}_2$ crosses the set $\{cz_2 + d = 0\}$ (dashed line, red), z_1^* and consequently u are no longer defined. To circumvent these problems, in the following section we redefine the virtual reference z_1^* such that (9) is satisfied.

5. HYBRID CONTROL DESIGN

To generate a signal z_1^* such that z_1 is PE, we propose the two-phase regulation logic defined in Fig. 4, wherein z_1^{ref}, χ_a, and χ_b are (tunable) design parameters. The system's associated phase-portrait is illustrated in Fig. 5. The idea behind this regulation logic is as follows.

- We assume that the initial condition of the system is such that $z_1 < 0$ and $z_2 < 0$. That is, we assume that the wheel has entered the unstable region of the tyre; if it goes too far into this region, the wheel will lock.
- During phase 1 the reference z_1^* is set to some positive value z_1^{ref}. The aim of this phase is to change the sign of the wheel acceleration offset and thus cause the wheel to return to the stable region of the tyre. Once z_1 becomes positive, z_2 starts to increase.
- As soon as z_2 crosses the threshold $\chi_b > 0$, phase 2 is triggered and the reference z_1^* is set to $-z_1^{\text{ref}}$. The aim of this phase is to prevent the wheel from going too far into the stable region, as this would result in a loss of friction force and thus in an increase of the braking distance. After the change of sign of z_1, the wheel goes back into the unstable region of the tyre and z_2 starts to decrease.
- As soon as z_2 crosses the threshold $\chi_a \leq 0$, phase 1 is triggered again and the cycle starts over.

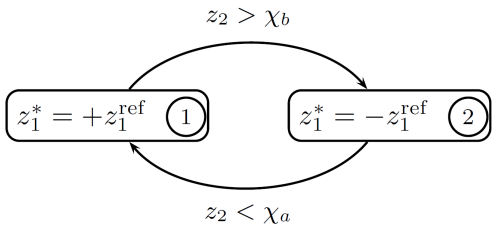

Fig. 4. Two-phase regulation logic for z_1^*. The switching of the reference is performed based on the value of z_2.

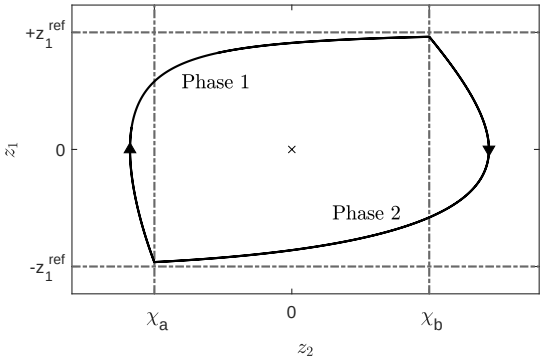

Fig. 5. Limit cycle associated to the regulation logic of Fig. 4. The aim of the algorithm is to keep the system oscillating around the origin.

The structure of this algorithm is similar to that of Corno et al. [2012], where the wheel acceleration is controlled to a positive or a negative reference during each phase using a proportional controller and the triggering of the phases is performed based on the measurement of the tyre longitudinal force. Nevertheless, unlike this approach we do not assume the availability of an additional sensor, hence the XBS observer is used instead.

The performance of the hybrid control algorithm of Fig. 4 is illustrated in Fig. 6. The graphics show the phase-plane evolution of the system when the control law is implemented using state feedback. The initial conditions of the system and the observer as well as the design parameters are the same as those used to evaluate the continuous control. Because of the new definition of z_1^*, note that in the implementation of this algorithm we drop the last term of u given by (3) as $\dot{z}_1^* = 0$ almost everywhere. In both cases the control drives the system to a limit cycle around the origin. Moreover, because z_1 is

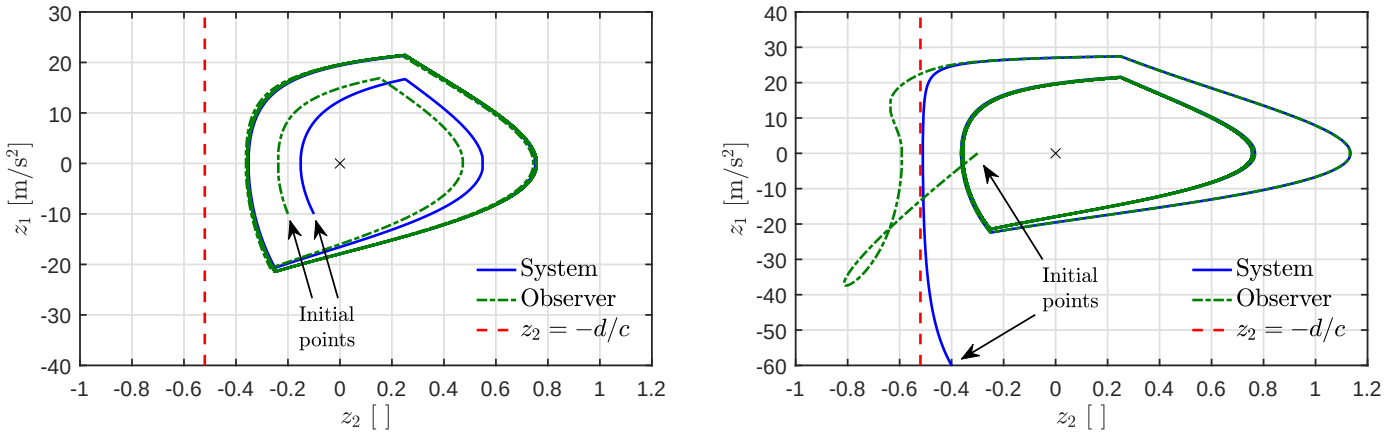

Fig. 6. Hybrid state-feedback control: the system converges to a limit cycle around the origin.

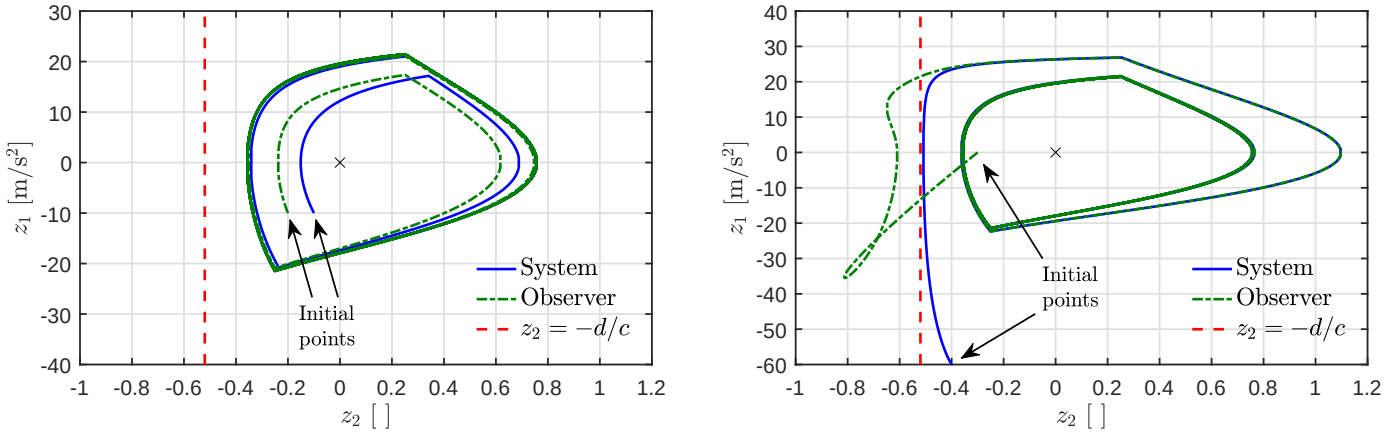

Fig. 7. Hybrid output-feedback control using XBS observer: the system converges to a limit cycle around the origin.

PE, the observer (implemented in open loop) converges to the true trajectories of the system.

Fig. 7 illustrates the performance of the hybrid control law when it is implemented using $\hat{z}_2$ instead of z_2. Even though the system is perturbed during the transient stage because of the initial estimation error, the estimated states converge to the true trajectories of the system. Moreover, the hybrid control shows robustness to $\hat{z}_2$ not staying within the feasible region. Hence, in all cases the control manages to drive the system towards a limit cycle around the origin, thus satisfying the control objective.

To assess the performance of the two-phase algorithm developed in this paper and compare it against that of an algorithm that use the same set of sensors, the five-phase algorithm of Pasillas-Lépine [2006] based on wheel deceleration thresholds is taken as a reference. A comparison between these two algorithms is illustrated in Fig. 8. The graphic shows the phase-plane evolution of the system in the wheel slip domain for a vehicle braking on wet asphalt with an initial speed of 120 km/h. The results obtained with different initial speeds and road conditions are summarised in Table 1, which shows the braking distance l_{brake} computed as

$$l_{\text{brake}} = \frac{v_x(0)^2}{2g\bar{\mu}},$$

where g denotes the gravitational acceleration and $\bar{\mu}$ is the average friction coefficient obtained in each scenario.

In all cases both algorithms manage to keep the system oscillating around the optimal braking point. With the two-phase algorithm, however, a smaller variation of the wheel slip with respect to its optimal value is obtained. In consequence, the average value of tyre-road friction coefficient is higher, and the braking distance is shorter than that of the five-phase algorithm. The reduction of the braking distance using the two-phase algorithm is especially noticeable at high speeds, in which a reduction of up to 1.5 meters is obtained.

Even though, theoretically, the operating interval around zero could be made arbitrarily small, in any real-time implementation the choice of the different design parameters cannot be made arbitrarily. For the algorithm to work properly, the thresholds χ_b and χ_a must take into account the (typical) maximum and minimum values of XBS that can be attained in a certain type of road, as well as the possible error in the estimate $\hat{z}_2$. The reference z_1^{ref} should not be too small, as this would cause the algorithm to be very sensitive to the measurement noise in the wheel acceleration offset. Moreover, the gain k_p should be sufficiently large in order to guarantee asymptotic stability of the limit cycle —see Aguado-Rojas [2019].

6. CONCLUDING REMARKS AND FUTURE WORK

We presented a hybrid control for ABS that uses XBS logic-based switching. Sufficient conditions to guarantee

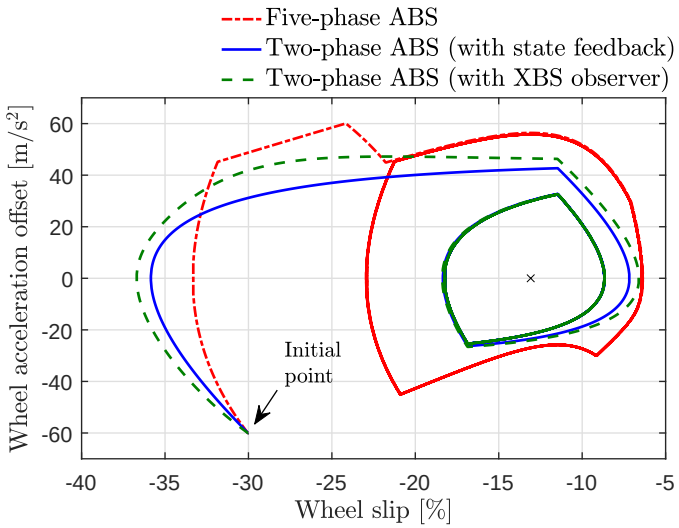

Fig. 8. Comparison between the two-phase algorithm and the five-phase algorithm of Pasillas-Lépine [2006]. The latter displays a larger variation of the wheel slip with respect to the optimal point.

the asymptotically stability of the limit cycle were established, provided that the wheel acceleration, the vehicle acceleration, and the XBS are known. Future work will focus on the stability analysis of the limit cycle including the XBS observer dynamics for the general case in which the road parameters are estimated as well. Future work will also consider the evaluation of the proposed algorithm in the presence of unmodelled dynamics such as load transfer, tyre relaxation, actuator delay, and changes in the brake efficiency and the road conditions.

Table 1. Braking distance: comparison between the two-phase and the five-phase algorithms.

Road condition	Braking distance [m]		
	Five-phase ABS	Two-phase ABS	Difference
Travelling speed: 60 km/h			
Dry asphalt	12.31	12.18	-0.13
Wet asphalt	18.09	17.86	-0.23
Dry concrete	13.24	13.08	-0.16
Dry cobblestones	14.34	14.28	-0.06
Wet cobblestones	38.46	38.30	-0.16
Travelling speed: 120 km/h			
Dry asphalt	49.27	48.78	-0.49
Wet asphalt	72.38	71.58	-0.80
Dry concrete	52.97	52.40	-0.57
Dry cobblestones	57.34	57.11	-0.23
Wet cobblestones	153.88	153.41	-0.47
Travelling speed: 180 km/h			
Dry asphalt	110.87	109.90	-0.97
Wet asphalt	162.88	161.37	-1.51
Dry concrete	119.27	118.10	-1.17
Dry cobblestones	129.01	128.51	-0.50
Wet cobblestones	346.08	345.57	-0.51

REFERENCES

Aguado-Rojas, M. (2019). *On control and estimation problems in antilock braking systems.* Ph.D. thesis, Université Paris-Saclay.

Aguado-Rojas, M., Pasillas-Lépine, W., and Loría, A. (2018). A switched adaptive observer for extended braking stiffness estimation. In *2018 American Control Conference (ACC)*, 6323–6328.

Burckhardt, M. (1993). *Fahrwerktechnik: Radschlupf-Regelsysteme.* Vogel-Verlag.

Choi, S.B. (2008). Antilock brake system with a continuous wheel slip control to maximize the braking performance and the ride quality. *IEEE Transactions on Control Systems Technology*, 16(5), 996–1003.

Corno, M., Gerard, M., Verhaegen, M., and Holweg, E. (2012). Hybrid abs control using force measurement. *IEEE Transactions on Control Systems Technology*, 20(5), 1223–1235.

Gerard, M., Pasillas-Lépine, W., de Vries, E., and Verhaegen, M. (2012). Improvements to a five-phase ABS algorithm for experimental validation. *Vehicle System Dynamics*, 50(10), 1585–1611.

Gustafsson, F. (1997). Slip-based tire-road friction estimation. *Automatica*, 33(6), 1087 – 1099.

Hoàng, T.B., Pasillas-Lépine, W., De Bernardinis, A., and Netto, M. (2014). Extended braking stiffness estimation based on a switched observer, with an application to wheel-acceleration control. *IEEE Transactions on Control Systems Technology*, 22(6), 2384–2392.

Kiencke, U. and Nielsen, L. (2005). *Automotive control systems: For engine, driveline, and vehicle.* Springer-Verlag Berlin Heidelberg, second edition.

Ono, E., Asano, K., Sugai, M., Ito, S., Yamamoto, M., Sawada, M., and Yasui, Y. (2003). Estimation of automotive tire force characteristics using wheel velocity. *Control Engineering Practice*, 11(12), 1361–1370.

Panteley, E. and Loría, A. (2001). Growth rate conditions for uniform asymptotic stability of cascaded time-varying systems. *Automatica*, 37(3), 453–460.

Pasillas-Lépine, W. (2006). Hybrid modeling and limit cycle analysis for a class of five-phase anti-lock brake algorithms. *Vehicle System Dynamics*, 44(2), 173–188.

Reif, K. (ed.) (2014). *Brakes, brake control and driver assistance systems: Function, regulation and components.* Bosch Professional Automotive Information. Springer Vieweg.

Singh, K.B., Arat, M.A., and Taheri, S. (2013). An intelligent tire based tire-road friction estimation technique and adaptive wheel slip controller for antilock brake system. *Journal of Dynamic Systems, Measurement, and Control*, 135(3), 031002.

Sugai, M., Yamaguchi, H., Miyashita, M., Umeno, T., and Asano, K. (1999). New control technique for maximizing braking force on antilock braking system. *Vehicle System Dynamics*, 32(4-5), 299–312.

Umeno, T. (2002). Estimation of tire-road friction by tire rotational vibration model. *R&D Review of Toyota CRDL*, 37(3).

Villagra, J., d'Andréa Novel, B., Fliess, M., and Mounier, H. (2011). A diagnosis-based approach for tire–road forces and maximum friction estimation. *Control Engineering Practice*, 19(2), 174 – 184.